Solution Structure, Stability, and Flexibility of Sso10a: A Hyperthermophile Coiled-Coil DNA-Binding Protein[†,‡]

Mebrahtu A. Kahsai, Bernhard Vogler, Andrew T. Clark, Stephen P. Edmondson, and John W. Shriver*

Biomolecular Nuclear Magnetic Resonance Laboratory, Laboratory for Structural Biology, Departments of Chemistry and Biological Sciences, Graduate Program in Biotechnology Science and Engineering, University of Alabama in Huntsville, Huntsville, Alabama 35899

Received November 2, 2004; Revised Manuscript Received December 15, 2004

ABSTRACT: Sso10a is one of a number of DNA-binding proteins from the hyperthermophile *Sulfolobus solfataricus* that has been associated with DNA packaging and chromatin regulation. Sequence analysis indicates that it is a member of a conserved group of archaeal transcription regulators (COG3432). We have determined the solution structure of Sso10a and show that it is a homodimer of winged-helix DNA-binding domains. The dimer interface consists of an extended antiparallel coiled coil, with the globular DNA-binding domains positioned at opposite ends of a solvent-exposed coiled-coil rod. NMR structure refinement of the elongated structure benefited not only from the inclusion of residual dipolar couplings from partially aligned samples but also the influence of anisotropic rotational diffusion on heteronuclear relaxation. An analysis of backbone mobility using ^{15}N relaxation rates indicated that the overall tertiary and quaternary structure is largely inflexible on the nanosecond to picosecond time scale. Amide hydrogen exchange data demonstrated that the most stable region of the protein extends from the core of the winged helices into the coiled coil. The positions of the globular heads relative to the coiled coil in solution deviate only slightly from that observed in a crystal structure. The most significant difference between the solution and crystal structures occurs in the putative DNA-binding helix-turn-helix (HTH) motif. This is the region of lowest stability in solution and a point of protein−protein contact in the crystal. Alternative conformations of the HTH motif may permit adjustment of the structure for optimal DNA binding.

The hyperthermophile *Sulfolobus* expresses a number of relatively abundant, small DNA-binding proteins that are thought to be involved in chromatin packaging and regulation of gene accessibility (*1*, *2*). Because of the relative simplicity and high thermal stability of these systems, they are especially attractive for structural thermodynamic studies of chromatin and DNA binding. Recent data indicate that regulation of chromatin organization and gene expression in the archaea may resemble that found in eukaryotes (*3*). It is noteworthy that the DNA-binding affinity of Sso10b, or Alba, is modulated by deacetylation by Sir2 (*2*). The monomeric 7-kDa Sac7d and Sso7d have been the best characterized members of this group, with detailed nuclear magnetic resonance (NMR), X-ray, and calorimetric studies of the proteins in solution as well as bound to DNA (*4*−*12*).

We have initiated studies of a third member of the *Sulfolobus* chromatin proteins known as Sul10a, with specific studies of Sac10a from *S. acidocaldarius* and Sso10a from *S. solfataricus* (*13*, *14*). Early electron micrograph studies demonstrated that native Sac10a bound to DNA forming "clumps" leading to super-twisting of closed circular DNA (*15*). Sedimentation equilibrium studies on Sac10a showed that the protein was dimeric and highly elongated (*13*). The coiled-coil prediction program COILS2 (*16*) indicated a strong tendency to form a coiled coil involving an extended C-terminal helix of 36 residues or 9 heptad repeats (38% of the sequence). Interestingly, initial attempts at crystallization of Sso10a resulted in crystals with fiberlike scattering patterns (*17*). This evidence indicated that Sso10a and homologous proteins might provide an opportunity to explore the structure and stability of a hyperthermophile coiled coil as well as DNA binding. We have therefore initiated a study of the structure of Sso10a using both X-ray crystallography and NMR. The crystal structure of Sso10a has been presented elsewhere (*14*), and we present the NMR solution structure here along with NMR data describing the distribution of stability and flexibility in the protein. The highly nonspherical structure of Sso10a has made it an excellent candidate for structural refinement using both residual dipolar couplings (RDCs)[1] as well as rotational diffusion anisotropy restraints obtained from ^{15}N relaxation data.

[†] This work was supported by Grant GM49686 from the National Institutes of Health to J.W.S. and S.P.E.

[‡] Coordinates for the solution structure of Sso10a have been submitted to the Protein Data Bank (accession number 1XSX).

* To whom correspondence should be addressed: Department of Chemistry, Materials Science Building, John Wright Drive, University of Alabama in Huntsville, Huntsville, AL 35899. Telephone: 256-824-2477. Fax: 256-824-6349. E-mail: shriverj@uah.edu.

[1] Abbreviations: C12E5, *n*-dodecyl-penta(ethylene glycol); CSI, chemical-shift index; D_a, axial component of the molecular alignment tensor; $D_{||}$, principal axis component of the molecular diffusion tensor; $D_{\perp}$, minor axis component of the molecular diffusion tensor in an axially symmetric system; DSC, differential-scanning calorimetry; NOE, nuclear Overhauser effect; PF, protection factor; *R*, rhombic component of the molecular alignment tensor for partially aligned samples; R_1,

10.1021/bi047669t CCC: $30.25
Published on Web 02/03/2005

MATERIALS AND METHODS

Protein Preparation. The gene for the Sso10a protein was identified in the genomic sequence of *S. solfataricus* (*18*) and was cloned and expressed as previously described in RossettaBlue (DE3) pLacI cells (Novagen) (*17*). *Escherichia coli* cells were grown at 37 °C, and protein expression was performed at 29 °C in standard LB medium. After induction with 1 mM ITPG, cells were incubated for 8 h and harvested by centrifugation and stored at −80 °C. Frozen cells were thawed, suspended in cold Tris-ethylenediaminetetraacetic acid (EDTA) buffer (10 mM Tris-HCl at pH 8.00, 10 mM EDTA at pH 8.00, 0.1% Triton X-100, and 0.5 mM PMSF), and lysed by sonication. A DNAse-I treatment was performed at 42 °C, and the lysate was incubated at 70 °C for 30−40 min to precipitate *E. coli* proteins. The crude extract was centrifuged at 300000*g*; the supernatant was filtered (0.45 μm filter) and loaded on an Amersham Hi-trap SP cation-exchange column in 10 mM KH_2PO_4 at pH 7.0; and the protein eluted with a linear NaCl gradient (0−1.0 M) at room temperature. Matrix-assisted laser desorption ionization time-of-flight mass spectrometry, sodium dodecyl sulfate−polyacrylamide gel electrophoresis, and N-terminal sequencing were used to confirm the identity of the protein. The N terminus showed no initiating methionine. The typical yield was 13 mg of protein/L of culture. Uniform ^{15}N- and ^{13}C,^{15}N-labeled protein were prepared by expression in minimal media containing $^{15}NH_4Cl$ as the sole nitrogen source and ^{13}C glucose as the sole carbon source in a 2 L Bioflo 3000 (New Brunswick, NJ) fermentor.

NMR Spectroscopy. NMR data for assignments and structure refinement were collected on Varian INOVA 500 MHz (11.7 T) and 800 MHz (18.7 T) NMR spectrometers with 5 mm triple resonance probes with pulse-field gradients (*z*-axis gradients on the INOVA 500 and triple-axis gradients on the INOVA 800). All NMR spectra were acquired with a sample temperature of 30 °C unless indicated otherwise (e.g., in partially aligned media). Samples were prepared by dissolving lyophilized protein in 700 μL of 90% H_2O/10% D_2O or 99.99% D_2O, and the pH was adjusted to 5.0 using a glass electrode with no correction for the deuterium isotope effect. The concentration of protein was approximately 10 mg/mL for spectra of ^{15}N-labeled protein and 25 mg/mL for ^{15}N,^{13}C-double-labeled protein. Sample concentrations were determined using an extinction coefficient ($A_{280nm}^{0.1\%}$) of 0.46 mL mg^{-1} cm^{-1}, calculated from the amino acid composition (*19*). Data processing was performed using VNMR (Varian, Palo Alto, CA), FELIX (Accelrys, San Diego, CA), or NMRPipe (*20*). Sequential assignments were made using NMRView (*21*) with in-house scripts adapted from those kindly provided by Dr. P. Legault (University of Georgia).

Sequential assignments were obtained using a combination of ^1H-^{15}N heteronuclear single quantum coherence (HSQC) and 3D HNCOCA, HNCA, HNCACB, and CBCA(CO)NH experiments at 18.7 T. Backbone carbonyl carbon resonances were assigned using 3D HNCO. Sequential amide proton assignments were confirmed using a 3D ^{15}N-edited nuclear Overhauser effect spectrometry (NOESY) spectrum (150 ms mixing time). Side-chain carbon and proton assignments were obtained using a combination of CCC-total correlation spectroscopy (TOCSY)-NNH, HCCH-TOCSY, and HCC-TOCSY-NNH spectra. An HBGCBGCCBGCACONNH (*22*) experiment was used to assign the side-chain carboxyl carbons of the acidic amino acids. $^3J_{HNH\alpha}$-coupling constants were obtained from an HNHA spectrum (*23*). Intramolecular ^1H-^1H nuclear Overhauser effects (NOEs) were obtained from both 3D ^{15}N-edited and ^{13}C-edited NOESY experiments (with 150 ms mixing times).

^{12}C-filtered, ^{13}C-edited NOESY spectra (150 ms mixing time) were acquired at 18.7 T to obtain intermolecular distance restraints as described elsewhere (*24*). Equal amounts (13 mg each) of ^{13}C,^{15}N-labeled and unlabeled Sso10a were mixed and unfolded through incremental addition of guanidinium hydrochloride to a final concentration of 6 M. Refolding was induced by a 10-fold dilution of the sample, and the denaturant was removed by extensive dialysis. The sample was lyophilized and dissolved in 99.99% D_2O for NMR data collection.

Amide hydrogen exchange data were collected using ^1H-^{15}N HSQC spectra collected at 18.7 T with 5 mg of lyophilized ^{15}N-labeled Sso10a dissolved in 700 μL of 99.9% D_2O in 10 mM potassium acetate at pH 7.0 and 30 °C with approximately 1 mM NaN_3. Spectra were collected on a sample stored at 30 °C over a period of 3 weeks with 45 min accumulation times for each spectrum. The time of protein−buffer mixing was recorded as the zero time of the exchange process.

^1H-^{15}N RDC measurements were made at 18.7 T using partially aligned ^{15}N-labeled Sso10a in a liquid crystalline media of *n*-alkyl-poly(ethylene glycol) and hexanol (*25*). Aligned samples were made in 90% H_2O/10% D_2O with 5% *n*-dodecyl-penta(ethylene glycol) (C12E5) (Sigma) with a C12E5/hexanol molar ratio (*r*) of 0.87. Aligned and unaligned spectra were obtained at 35 and 45 °C, respectively. Single-bond ^1H-^{15}N RDCs were obtained using the Varian BioPack ^1H-^{15}N HSQC-IPAP pulse sequence. Raw data sets contained 512 data points in the ^1H dimension and 256 increments in the ^{15}N dimension. Data were linear-predicted by a factor of 2 in the ^{15}N dimension and zero-filled to obtain 1024 × 1024 (^1H × ^{15}N) data points in the final spectrum. RDCs were extracted using in-house NMRView scripts.

{^1H}^{15}N NOE, and ^{15}N longitudinal relaxation time (T_1) and rotating frame relaxation time ($T_{1\rho}$) measurements were performed at 11.7 T using sensitivity-enhanced-gradient selected HSQC pulse sequences (*26*, *27*). ^1H saturation for {^1H}^{15}N NOEs was obtained using a series of 120° ^1H pulses with 5 ms separation. Saturation was performed for 5 s, with a total recycle delay of 10 s for both saturated and unsaturated experiments. Suppression of cross-correlation effects in ^{15}N $T_{1\rho}$ experiments was obtained using a train of phase alternated, random length ^1H continuous wave pulses applied during the ^{15}N spin lock (*27*). T_1 delay times were 0.09, 0.18, 0.29, 0.40, 0.52, 0.66, 0.81, 0.99, and 1.2 s. $T_{1\rho}$ delay times were 0.01, 0.02, 0.03, 0.04, 0.05, 0.06, and 0.08 s. Duplicate {^1H}^{15}N NOE experiments and duplicates of ^{15}N T_1 and $T_{1\rho}$ experiments at three different delay times were used to estimate uncertainties in peak intensities. T_1 and $T_{1\rho}$ data were fit with the CURVEFIT module of MODELFREE (*28*). Transverse relaxation rates (R_2) were calculated from $R_{1\rho}$ rates as described by Korzhnev et al. (*27*). The errors in

longitudinal relaxation rate ($1/T_1$); R_2, transverse relaxation rate ($1/T_2$); RDC, residual dipolar coupling; rmsd, root-mean-square deviation; τ_m, overall rotational correlation time; T_1, longitudinal relaxation time; $T_{1\rho}$, rotating frame relaxation time; T_2, transverse relaxation time.

measured longitudinal relaxation rate (R_1), R_2, and NOE values were 0.03, 0.22, and 0.03, respectively.

Structure Calculation. Initial unambiguous ^{1}H-^{1}H NOE assignments (180 total) were obtained manually using NMRView (*21*). Subsequent NOE peak assignments were achieved semiautomatically using ARIA (version 1.2) (*29*) interfaced to CNS (version 1.1) (*30*). In each ARIA iteration, distance restraints were calibrated and NOE assignments were refined based on an ensemble of the lowest energy structures from the previous iteration. A preliminary structure of a monomer of Sso10a was computed using ARIA/CNS starting from a random chain. Input to ARIA consisted of ^{15}N-edited NOESY and ^{13}C-edited NOESY cross-peak lists, 144 dihedral angle restraints generated from chemical-shift indices (CSI), and 88 ambiguous hydrogen bonds generated from CSI values. Default values of the CNS torsion-angle molecular dynamics parameters were used with an initial equilibration temperature of 10 000 K followed by cooling stages to 1000 K and then 50 K. The resulting structures showed a globular fold for residues 1−60 in good agreement with single monomers in the unit cell of the crystal structure, which was determined simultaneously in collaboration with Dr. Liqing Chen (*14*). Preliminary monomer structures along with amide hydrogen exchange data allowed the identification of 41 intramolecular hydrogen bonds that were used as input restraints for further refinement. An extended C-terminal helix predicted by CSIs was observed to fold onto itself in the monomer structures generated from the NMR restraints. This helix was previously predicted to form a two-stranded coiled coil using COILS2, and ultracentrifugation data confirmed that the protein was dimeric in solution (*13*, *14*).

Measured RDCs were found to be in good agreement with those calculated with REDCAT (*31*) using dimeric Sso10a generated from the crystal data. The crystal structure was therefore used as an initial structure for refinement of the dimer in solution using NMR restraints with ARIA/CNS, which was modified to permit refinement of homodimers (B. Jordan, personal communication). Input consisted of the same ^{1}H-^{1}H NOEs used for the monomer refinement described above plus noncrystallographic symmetry restraints to enforce a symmetric dimer, RDCs (52 per monomer), hydrogen bonds defined by hydrogen−deuterium exchange (41 per monomer), and unambiguous intermolecular NOEs assigned from a ^{12}C-filtered, ^{13}C-edited NOESY spectrum (34 per dimer). Intermolecular NOE restraints were recalibrated during each ARIA iteration, but ARIA was not permitted to reassign them. Initial estimates of the axial and rhombic components of the RDC tensor were calculated from the dimer crystal structure using REDCAT (viz. axial component of the molecular alignment tensor (D_a) = 12.3 Hz, and rhombic component of the molecular alignment tensor for partially aligned samples (R) = 0.29). Simulated annealing was performed in CNS using Cartesian molecular dynamics with an initial temperature of 1000 K using the default parameters. The force constant for dipolar coupling restraints was ramped from 0.1 to 1.0 during simulated annealing. All ambiguous distance restraints with contributions from other atom pairs besides those of the symmetry-related subunit were deleted from the final set of restraints determined by ARIA, and these were used for Xplor-NIH refinement.

Refinement of the dimer structure using Xplor-NIH (*32*) (version 2.9.6) included intra- and intermolecular NOE, dihedral angle, coupling constant, and hydrogen-bond restraints. Three additional sets of refinements were performed using (1) ^{15}N T_1/transverse relaxation time (T_2) data, (2) RDCs, and (3) both RDC and ^{15}N T_1/T_2 restraints. T_1 and T_2 relaxation times were used for restraints for only those amide nitrogens (54 total) that were (1) in a defined secondary structure indicted by the refinement up to this point and (2) did not fall in suspected mobile regions as indicated by significantly low {^{1}H}^{15}N NOEs. Xplor-NIH internal dynamics were used with an initial equilibration at 3000 K, slow cooling to 100 K with 50 K temperature decrements, followed by energy minimization. During both the equilibration and cooling phases, distance restraint force constants were increased from 5 to 50 kcal/mol, and force constants for dipolar coupling and T_1/T_2 restraints were increased during the cooling phase from 0.01 to 1.0 and 0.5 to 5.0, respectively. For refinements that included dipolar coupling and/or T_1/T_2 restraints, a grid search was implemented at each temperature change during the simulated annealing to find optimal values of D_a, $D_{\parallel}/D_{\perp}$ (i.e., the ratio of the principal and minor axis components of the molecular diffusion tensor), R (rhombicity), and the overall rotational correlation time (τ_m). The final values characterizing the molecular alignment tensor were a D_a of 16.0 Hz and a rhombicity of 0.24. The rotational diffusion anisotropy defined by the T_1/T_2 restraints converged to a $D_{\parallel}/D_{\perp}$ of 2.0 with a rhombicity of 0.05 and an overall τ_m of 13.7 ns.

The 10 lowest energy structures from Xplor-NIH refinements were used to define an ensemble of NMR structures obtained for each refinement protocol. An average structure for each ensemble was obtained by averaging the coordinates of the structures in each and subjecting these to restrained energy minimization. In addition, a representative structure was chosen from each ensemble based on the lowest backbone root-mean-square deviation (rmsd) relative to the average structure. The quality of the final structures was analyzed using PROCHECK-NMR. The coordinates and resonance assignments have been deposited in the Protein Data Bank (PDB 1XSX) and the BioMagResBank (BMRB 5891).

{^{1}H}^{15}N NOE and ^{15}N Relaxation Data Analysis. {^{1}H}^{15}N NOE and ^{15}N T_1 and T_2 relaxation data were analyzed using MODELFREE4 with an axially symmetric anisotropic rotational diffusion model. Values for $D_{\parallel}/D_{\perp}$ (2.09) and the overall rotational correlation time τ_C (13.8 ns) were obtained by optimization of the global diffusion model using only those ^{1}H,^{15}N pairs in defined secondary structure with {^{1}H}^{15}N NOEs at the upper extreme of the observed range. Order parameters were determined using MODELFREE4, with model selection made using 95% confidence limits, as described in the software manual.

Amide Hydrogen Exchange Analysis. Amide hydrogen−deuterium exchange was followed with ^{1}H-^{15}N HSQC spectra at 18.7 T. Peak intensities were quantified by a 3 × 3 points volume integration using FELIX, and the time dependence of the volumes was fit to a general first-order exponential function $V(t) = a + b(1 - \exp(-k_{ex}x))$ to obtain the exchange rate constants, k_{ex}. The intrinsic rate constant of exchange, k_{int}, for each amide proton at the pH and temperature of the experiment was calculated as described elsewhere (*33*).

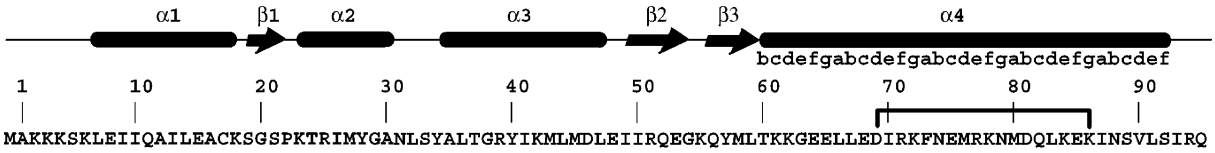

FIGURE 1: Amino acid sequence of recombinant Sso10a with α-helix (cylinders) and *β*-strand (arrows) secondary structure derived from the NMR solution structure. The heptad repeat assignment from COILS2 and verified by the NMR structure is indicated below helix α4. The bold bracket indicates the locations of D69 and K86, which are involved in intermolecular interactions with K86′ and D69′, respectively, of the other monomer at the coiled-coil interface.

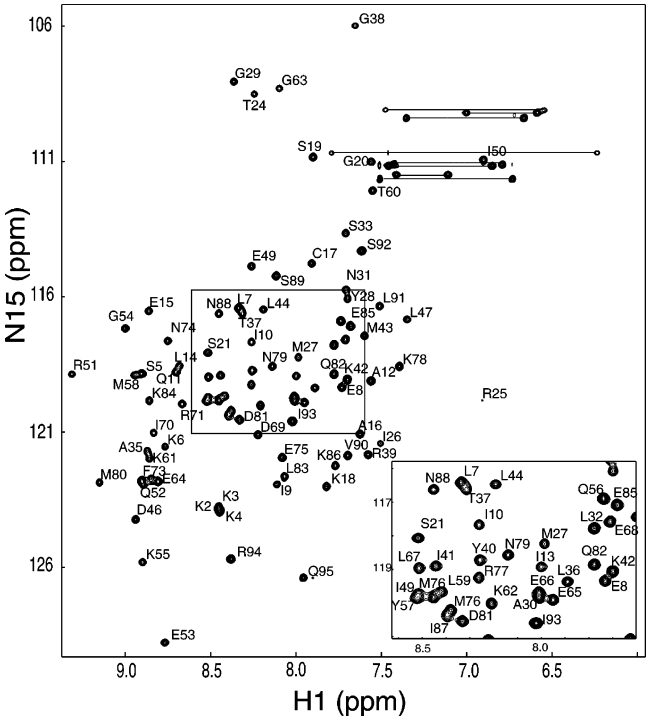

FIGURE 2: ^{1}H-^{15}N HSQC spectrum of Sso10a at pH 5.0 and 30 °C. Sequential assignments are indicated adjacent to each peak. Asparagine and glutamine side-chain correlations are indicated with horizontal lines. The crowded central region of the spectrum (enclosed by the box) is expanded in the inset at the lower right.

RESULTS

Resonance Assignments and Secondary Structure. Sso10a is a highly basic DNA-binding protein with a calculated pI of 9.75 (13 lysines, 7 arginines, 9 glutamates, 3 aspartates, and no histidine) and a molecular mass of 11.1 kDa for the 95 residue monomer chains (Figure 1). Under low-salt conditions, a well-resolved ^{1}H-^{15}N HSQC spectrum of Sso10a was obtained at 18.7 T with 90 of the expected 93 HSQC peaks resolved (Figure 2**)**. The protein contains a single proline. Cross peaks for K2, K3, and K4 were overlapping, and M45 could not be observed. Three residues showed unusually intense ^{1}H-^{15}N cross peaks, and these proved to originate from C-terminal residues (I93, R94, andQ95) with significant flexibility demonstrated by ^{15}N relaxation studies (see below). K23 and Y34 gave very weak cross peaks in ^{1}H-^{15}N HSQC spectra. Backbone assignments (98% complete) were obtained using a standard set of triple resonance experiments (HNCA, HN(CO)CA, HNCACB, CBCA(CO)NNH, and HNCO), and side-chain ^{1}H and ^{13}C assignments (82% complete) were obtained with CCC-TOCSY-NNH, HCCH-TOCSY, and HCC-TOCSY-NNH. It was not possible to unambiguously assign aromatic ring ^{1}H and ^{13}C resonances because of significant cross-peak overlap. CSI analysis of H^{α}, C^{α}, C^{β}, and C′ chemical shifts indicated extensive secondary structure with four α-helical segments (L7-K18, K23-G29, S33-46D, and K61-V90) and two *β* strands (50I-53E and Q56-T60).

Tertiary and Quaternary Structure. NMR restraints were used to define an initial monomer structure with ARIA/CNS, which contained a well-defined globular domain with a winged helix fold. The C-terminal α4 helix was not well-defined in these initial refinements, possibly because of incorrect assignments by ARIA of intermolecular cross peaks to intramolecular interactions. CSIs indicated that the C terminus from K61 to V90 was an extended helix, which was predicted to form a coiled coil using COILS2. Because dimer formation was indicated by both ultracentrifugation and differential scanning calorimetry (DSC), it was concluded that dimerization most likely resulted from the predicted coiled coil (*14*). A parallel coiled coil seemed unlikely given the presence of D69 in the *d* position of the predicted heptad repeat pattern (Figure 1). ^{12}C-filtered, ^{13}C-edited NOESY data using a mixture of unlabeled and ^{13}C-labeled Sso10a supplied intermolecular ^{1}H-^{1}H NOEs, which demonstrated that dimerization in solution resulted from formation of an antiparallel coiled coil. This was confirmed by a crystal structure determined in collaboration with Dr. L. Chen, which showed a single monomer in each unit cell with packing of adjacent extended α4 helices in an antiparallel orientation (*14*). Finally, ^{1}H-^{15}N RDCs for Sso10a in solution were in good agreement with those calculated using REDCAT from the crystal structure of the dimer with an antiparallel coiled coil. The dimer structure obtained from X-ray crystallography was therefore used as an initial structure for refinement using only NMR restraints (see the Materials and Methods). The final refinement with Xplor-NIH included 1231 intramolecular and 83 intermolecular distance restraints, 144 torsion-angle and 41 hydrogen-bond restraints, 52 RDCs, and 54 T_1/T_2 ^{15}N relaxation time measurements (Figure 3). For comparison, structures were also determined without RDCs and ^{15}N relaxation data, and these will be discussed below after describing the structure obtained from the complete set of restraints. Refinement statistics are summarized in Table 1. An ensemble of the 10 lowest energy structures (Figure 4A) showed an rmsd of 0.56 Å over the backbone secondary structural elements and 1.10 Å for all backbone atoms (C^{α}, C′ and N). A ribbon diagram of the structure with the smallest rmsd to the average NMR structure is shown in Figure 4B, along with the major and minor axes of the molecular alignment and rotational diffusion tensors.

The refined NMR solution structure of dimeric Sso10a contains two globular winged helix domains separated by a solvent-exposed, two-stranded antiparallel coiled-coil rod. The globular heads contain three helices, α_1 (L7-K18), α_2-(K23-A30), and α_3 (Y34-L47), with potentially a short *β* strand (β_1, S19-S21) connecting the first and second helices.

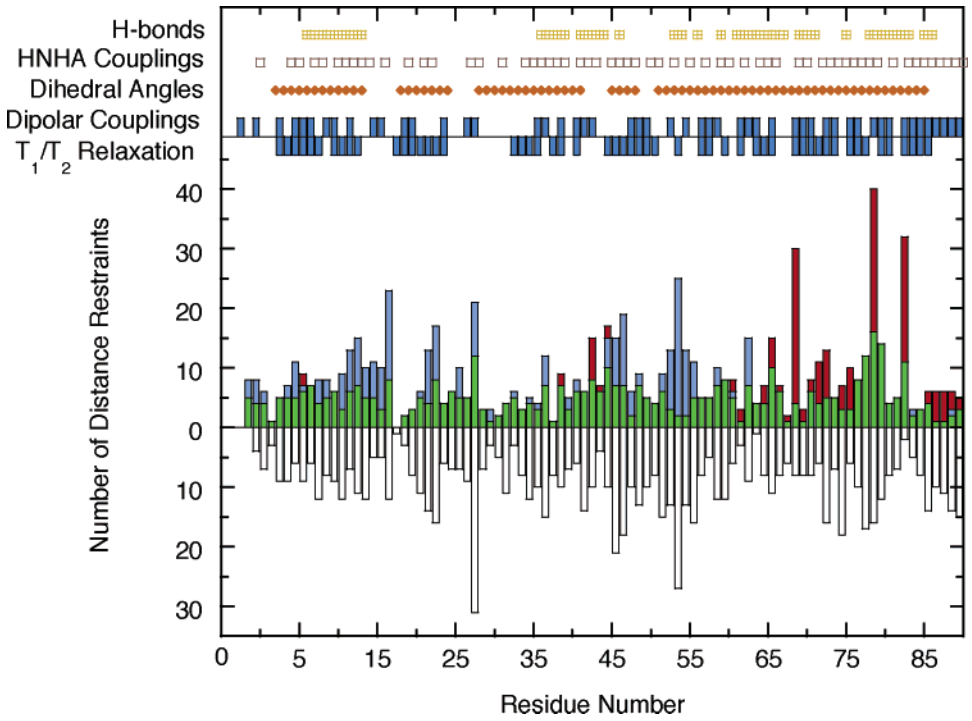

FIGURE 3: Sequential distribution of NMR restraints used to define the solution structure of Sso10a. (Top) hydrogen bonds, $^3J_{HNH\alpha}$ coupling constants, dihedral angles from CSIs, ^{1}H-^{15}N RDCs, and T_1/T_2 ratios from ^{15}N relaxation data. (Bottom) Number of ^{1}H-^{1}H NOEs per residue, showing intraresidue NOEs (open bars), medium-range (green bars) and long-range (blue bars) interresidue NOEs, and intermolecular monomer−monomer NOEs (red bars) obtained from a ^{12}C-filtered, ^{13}C-edited NOESY spectrum of a 50:50 mixture of uniformly ^{13}C-labeled and unlabeled Sso10a.

Table 1: Statistics for the Refinement of the NMR Solution Structure of Sso10a

coordinate rmsd (Å)	
backbone (2° structure only)	0.56
backbone (all residues)	1.10
all heavy atoms	1.49
number of restraint violations[a]	
NOE distances > 0.5 Å	2.0
torsional angles > 10°	4.6
$^3J_{HNH\alpha}$ > 1 Hz	50.7
rmsd of basic restraint violations	
distance restraints (Å)	0.06
torsional angles (deg)	2.49
$^3J_{HNH\alpha}$ (Hz)	1.25
rmsd of alignment and rotational diffusion restraint violations	
dipolar coupling (Hz)	1.02
T_1/T_2 relaxation	0.77
rmsd from ideal geometry	
bonds (Å)	0.003
angles (deg)	0.52
impropers (deg)	0.54
Ramachandran plot statistics (%)	
most favored	77.7
allowed	15.3
generously allowed	4.9
disallowed	2.1
rmsd between NMR and X-ray structures (Å)[b]	
dimer	2.16
monomer	1.41
coiled coil	1.11
winged helix	1.19

[a] The number of restraint violations for the NMR structures was averaged over the ensemble of best structures, and therefore values are not integers. [b] rmsd between the backbone atoms of the average NMR structure and the X-ray crystal structure.

These are followed by a two-stranded β ribbon (the "wing") composed of β_2 (I49-E53) and β_3 (Q56-L59). The extended strand (which we will refer to as β1) between helices α1 and α2 lies adjacent to the wing and may form a three-stranded β sheet with the wing with one hydrogen bond indicated by the structure. A fourth helix, α_4 (T60-S92), immediately follows the wing and extends 45 Å with at least eight turns. The α4 helix leads to dimerization through formation of an antiparallel coiled coil with another monomer. The distance between the distal ends of the two wings defined by the G54 C^α in each monomer is 77 Å, and the distance between centers of the α3 helices (defined by the R39 C^α in each) is 53 Å. A natural twist conferred by the coiled coil results in a relative angle between the α3 helical axes of the two globular subdomains of about 70°.

The sequence dependence of the backbone rmsd of the 10 structures in the lowest energy ensemble indicates that the greatest imprecision occurs at the N and C termini and also at the transition from the α2 to α3 helices. The pronounced decrease in backbone rmsd values over the coiled coil (Figure 5A) is at least in part due to the alignment of a set of prolate ellipsoids.

Overall Correlation Time and Rotational Diffusion Anisotropy. The Sso10a dimer is highly elongated with approximately a 2:1 major to minor axis ratio. Structure refinement with Xplor-NIH with ^{15}N T_1/T_2 ratios resulted in a rotational diffusion tensor characterized by a $D_\parallel/D_\perp$ of 2.0 and a rhombicity of 0.05 with an overall rotational correlation time τ_m of 13.7 ns. The low rhombicity demonstrates that the anisotropic rotational diffusion can be assumed to be axially symmetric. Optimization of the global diffusion model in MODELFREE4 using ^{15}N relaxation data and an axially symmetric anisotropic diffusion model resulted in an overall rotational correlation time τ_m of 13.8 ns and a rotational diffusion anisotropy characterized by a $D_\parallel/D_\perp$ of 2.09.

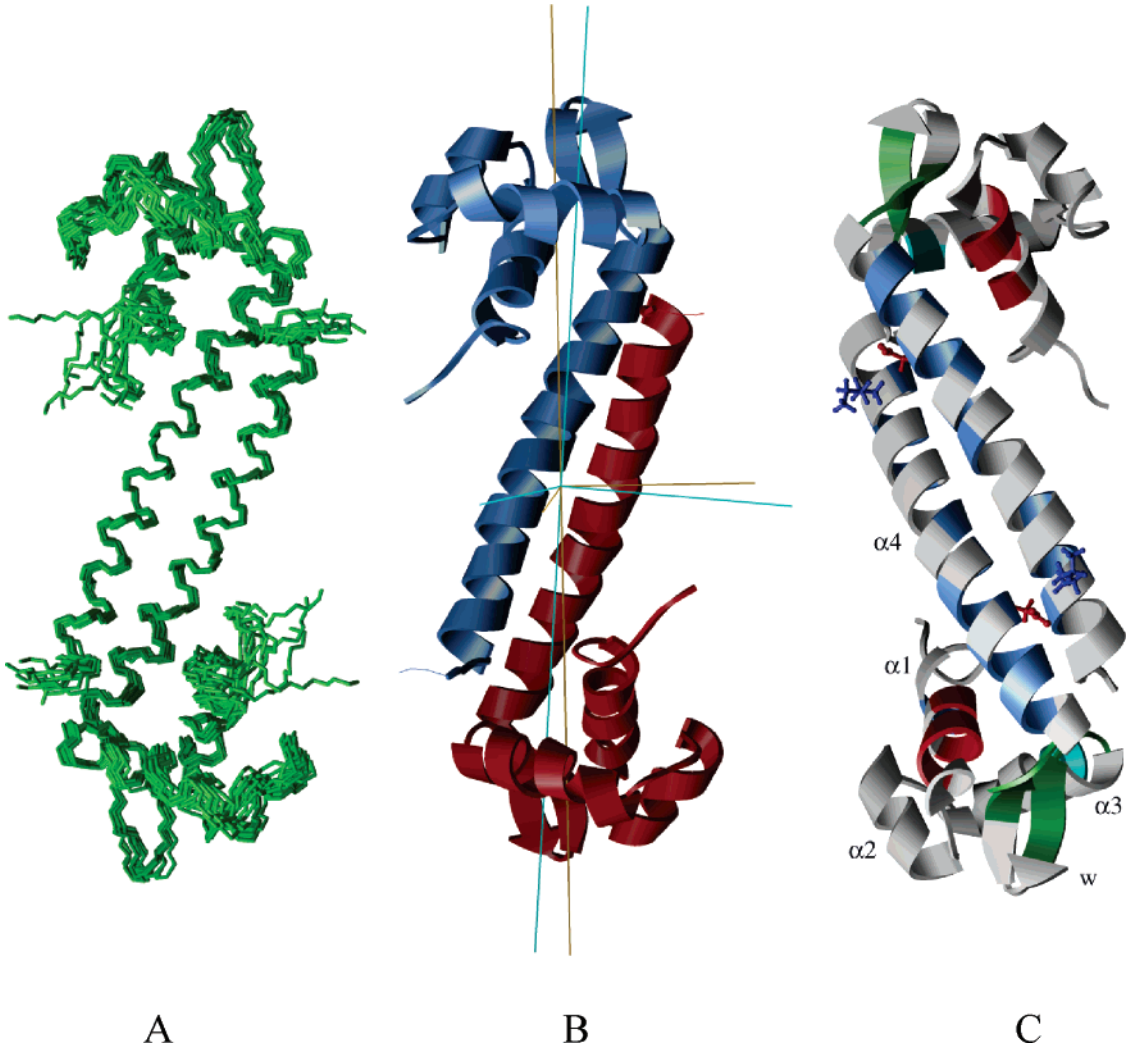

FIGURE 4: NMR solution structure of dimeric Sso10a. (A) Overlay of an ensemble of the 10 lowest energy NMR structures defined by Xplor-NIH with NOE distance restraints, CSI, amide hydrogen exchange, $^{3}J_{HNH\alpha}$ coupling constants, RDCs, and T_1/T_2 ^{15}N relaxation data. Structures were aligned using the backbone atoms in secondary structural segments (residues 8−18, 23−29, 31−46, 50−53, 56−59, and 61−91), (B) Ribbon drawing of the structure with the smallest rmsd to the average NMR structure. The viewing angle is the same as in A. The molecular alignment (gold) and diffusion (blue) tensor axes are shown for comparison. (C) Ribbon drawing of Sso10a showing the location of the slowly exchanging amide protons characterized by PFs of 10^5 or greater. The molecule is rotated 180° about the long axis relative to that in A and B. Color is used to highlight stable regions within specific secondary structural elements: α1 (red), C-terminal end of α3 (cyan), the "wing" (green), and coiled coil (blue). The side chains of D69 (red) and K86 (blue) are displayed using ball-and-stick representations to demonstrate their locations at the coiled-coil interface. Helices α1−α4 and the "wing" (w) are labeled in C.

The ^{15}N T_1/T_2 ratios for Sso10a (Figure 5) occur in four distinct blocks encompassing residues 5−20, 25−33, 34−60, and 61−91, with the most prominent difference occurring for the last two. The T_1/T_2 ratios for residues 34−60 are relatively constant at about 12, followed by an average of about 20 for residues 61−91. Residues 34−60 encompass helix α3 and the β-ribbon "wing", both of which have N−H vectors oriented largely perpendicular to the major axis of the diffusion tensor of the dimer. These vectors experience the most rapid rotational motion in the molecule because of rotation about the long axis of the dimer and therefore exhibit the smallest T_1/T_2 ratio. The exception in this region is residue 48, which lies at the transition from α3 to the β-ribbon wing, and the N−H vector is almost parallel to the long axis. Residues 61−91 define the coiled coil, and the N−H vectors are aligned roughly parallel to the major axis of the diffusion tensor. As a result, they experience slower rotation about the minor axes. Note that the dispersion in the T_1/T_2 values over this region is not due to noise (compare to the 34−60 data) but is due to the fact that N−H vectors deviate by about 13° from the axis of an α helix. Because the helices wrap around the long axis of the coiled coil, some of the N−H vectors are aligned closer to the major tensor axis, while others deviate significantly away from the axis. The oscillation in T_1/T_2 values was fit well by the refinement using the relaxation data as restraints (Figure 5). Similarly, the T_1/T_2 ratios for segments 5−20 and 25−33 can be correlated with the angle that the respective helices (α1 and α2) make with the major diffusion axis, with the α1 axis nearly midway between that for α3 and α4 and the α2 axis similar to that of α4.

Internal Mobility and Model-Free ^{15}N Relaxation Analysis. The Lipari−Szabo model-free formalism (*34*) was used to analyze backbone flexibility in Sso10a at 30 °C. ^{15}N relaxation data for 71 of the amide nitrogens were fit using MODELFREE4 with an axially symmetric diffusion model. Relaxation of half ($^{35}/_{71}$) of the N−H vectors could be fit to model 1 in MODELFREE, which assumes that relaxation is

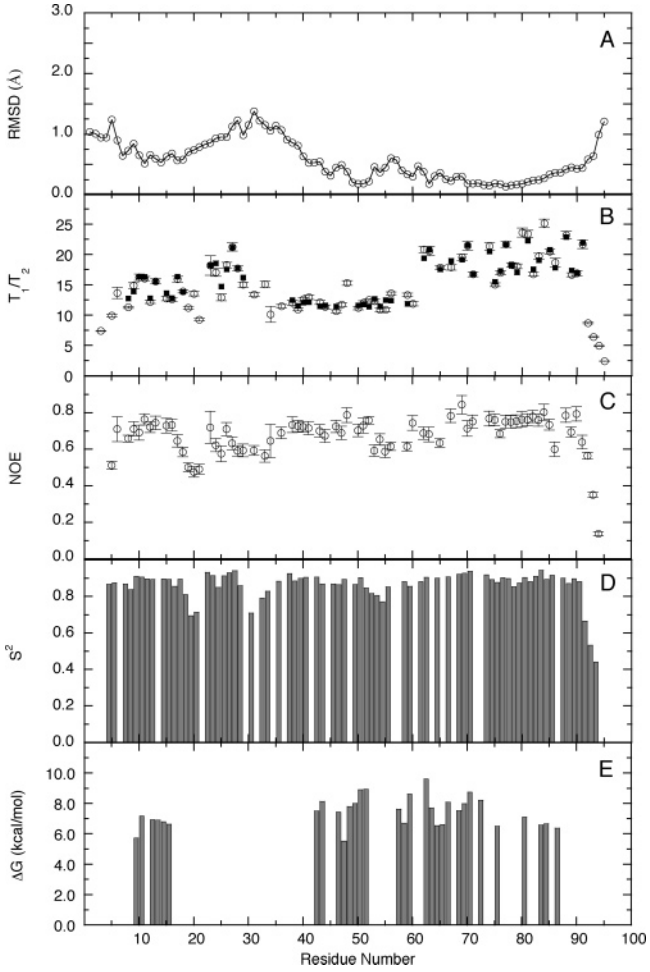

FIGURE 5: Sequence-dependent properties of Sso10a structure. (A) Average backbone rmsd of the ensemble of the 10 best structures relative to the average structure aligned using well-ordered secondary structure regions (see Figure 4). (B) Experimental T_1/T_2 ratios (○) [error bars indicate ±1 standard deviation (SD)] and those calculated from the NMR structure closest to the ensemble average (■). Calculated values are shown only for those T_1/T_2 ratios that were used for structure refinement. (C) $\{^1H\}^{15}N$ NOE values with error bars indicating ±1 SD (D) Generalized order parameter S^2 calculated from ^{15}N relaxation data using MODELFREE as described in the text. (E) Estimated free energies of local unfolding obtained from $-RT$ ln(PF), where amide proton PFs were measured from amide hydrogen−deuterium exchange rates.

defined by a generalized order parameter S^2, an overall rotational correlation time τ_m, and the rotational anisotropy parameters obtained from optimization of the global diffusion model described above. The majority of the remaining N−H vectors were fit with model 2 of MODELFREE, which includes an additional contribution from internal motions on the picosecond time scale with a correlation time τ_e. Only 4 N−H vectors required model 3 with the inclusion of an R_{ex} contribution due to microsecond to millisecond motions (residues 9, 52, 79, and 80). Flexible regions in Sso10a are indicated by the order parameters and the $\{^1H\}^{15}N$ NOEs shown in Figure 5. The average order parameter for the secondary structure regions was 0.89 overall, with separate elements having averages of 0.88 (α1), 0.91 (α2), 0.89 (α3), 0.90 (α4), 0.85 (*β*1), 0.85 (*β*2), and 0.87 (*β*3). It is noteworthy that S^2 throughout α2 and α3 helices was consistently high (>0.85) and that all of the data in this region could be fit with either model 1 or 2. There was no

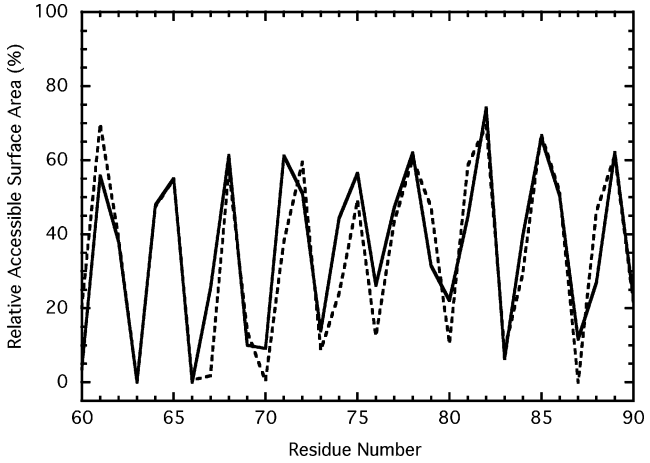

FIGURE 6: Solvent-accessible surface area of the side chains in helix α4 of Sso10a. The accessible surface area of the side chain in the NMR solution structure (—) is indicated as the percentage of that observed in a tripeptide AXA calculated with Naccess using a water probe of 1.4 Å. For comparison, the results calculated using the crystal structure of Sso10a (1R7J) are also shown (- - -).

evidence for slow motions on the millisecond to microsecond time scale in these helices. The more flexible regions indicated by lower order parameters occurred in the vicinity of G20 (S^2 of 0.70), N31 (S^2 of 0.71), and at the C terminus (L91, S92, and I93). Motions in the vicinity of G20 indicate that the *β*1 strand does not form a stable three-stranded sheet with the *β*2−*β*3 wing. This is also supported by amide hydrogen exchange data (see below). The increased flexibility in the vicinity of A30 occurs in the loop between α2 and α3, indicating that this portion of the helix-turn-helix (HTH) motif is not rigid in solution. A smaller increase in flexibility was noted around G54, which coincides with the loop separating the two strands of the wing. The high S^2 values observed from T60 to V90 indicate the absence of significant flexibility in the solvent-exposed regions of the coiled coil in the millisecond to picosecond time scale. The order parameters in the vicinity of the unusually located D69 were the highest observed, ranging from 0.91 to 0.94. All of the data in this region was fit with model 1. S^2 for G63 was 0.91, and the relaxation data for this N−H was also fit with model 1.

Hydrophobic Core and Domain Organization. Helix α1 is packed against the coiled coil with hydrophobic side chains donated by L7, Q11, and L14. In addition, I9, I10, I13, and C17 form a hydrophobic interface with α2 and α3 to define a hydrophobic core with I26, L32, I41, L44, L47, I49, and I50. The wing is largely composed of hydrophilic residues except at the end where L59 is solvent-exposed prior to the beginning of the coiled-coil α4 helix with K61. L66, L67, and I70 at the N-terminal region of the α4 form a hydrophobic interface with the globular heads. The solvent-accessible surface areas of the side chains in the α4 helix show a characteristic 4−3 periodicity (Figure 6), which reflects the hydrophobic *a*−*d* periodicity of the coiled-coil heptad (*35*−*37*). The *a* and *d* residues are hydrophobic except for D69 (with a solvent accessibility of 10% relative to an extended chain). Finally, L91 at the C terminus of the coiled-coil helices is inserted into the hydrophobic interface with the second winged helix subdomain. The hydrophobic core

of the coiled coil at its two ends is packed against the hydrophobic cores of the two winged helices so that the cores are continuous. The structure is consistent with a single cooperative domain, rather than separate winged helix and coiled-coil domains.

Amide Hydrogen Exchange and Cooperative Core Residues. The most stable core residues in Sso10a were defined by native-state hydrogen exchange. A total of 31 amide protons were observed to exchange in D_2O over a period of 3 weeks at pH 7.0 and 30 °C (Figure 5). The most stable regions of the molecule included many of the residues in the α1 helix (red, Figure 4C) with protection factors (PFs) on the order of 10^5, corresponding to a ΔG of unfolding of about 7 kcal/mol (assuming EX2 exchange). In addition, the C terminus of α3 (cyan) as well as the base of the "wing" (green) and a significant portion of the antiparallel coiled coil (blue) showed PFs from 10^5 to nearly 10^7 and ΔG values for unfolding on the order of 7−9 kcal/mol. Less stable regions indicated by complete amide exchange in less than an hour following mixing at pH 7 included the amino terminus, as well as the HTH motif including all of α2, the turn between α2 and α3, and a significant portion of α3. The N−H of G63 was the most protected, with a log(PF) of 6.93 or a ΔG of 9.61 kcal/mol. G63 is at the N terminus of α4 and lies at the interface with the winged helix subdomain. About half of the amide protons in α4 showed significant PFs, with the level of protection reflecting a periodicity similar to that observed for solvent accessibility (Figure 6). Free energies of unfolding for the protected protons in the helix showed that the stability of the coiled coil was comparable to that of the winged helices. This is consistent with the observation of a single endotherm in the thermal unfolding of Sso10a (*14*) and indicates that the protein folds as a single cooperative domain, i.e., the coiled-coil and winged helices are not separate cooperative domains.

Benefit of RDC and Rotational Diffusion Anisotropy Restraints. The advantages conferred by RDC and ^{15}N relaxation data in defining the Sso10a NMR structure were investigated by performing separate refinements using the basic set of NMR restraints (NOE distance, dihedral angles from CSI, $^3J_{HNH\alpha}$, and hydrogen-bond restraints) with and without RDC and ^{15}N T_1/T_2 restraints. The results are summarized here with details provided in tabular form in the Supporting Information.

As noted above, there was a significant correlation between the measured dipolar couplings and those calculated from the X-ray structure with a correlation coefficient of 0.91 and a root-mean-square error of 6.4 Hz. The structures determined using only the basic NMR restraints exhibited a slightly higher error of 8.7 Hz. As expected, agreement between measured and calculated dipolar couplings improved significantly when dipolar coupling restraints were included in the refinement (rmsd of 0.7). A good fit of dipolar couplings was also obtained when both RDCs and relaxation restraints were used. Interestingly, refinements using dipolar couplings do not improve fits of the T_1/T_2 ratios, and using T_1/T_2 restraints did not improve the agreement with dipolar couplings.

RDCs significantly increased the precision of the structure in terms of the rmsd values of the ensemble of the lowest energy structures. Only marginal improvement was obtained from also including T_1/T_2 ratios, possibly because of the greater rhombicity of dipolar interactions in the alignment media. The diffusion anisotropy of Sso10a was axially symmetric ($R = 0.05$), and there was no information in the ^{15}N relaxation data on the distribution of N−H vectors about the long axis of the molecule. In contrast, dipolar coupling showed significant rhombicity (0.24), and better convergence was obtained when the dipolar couplings were included.

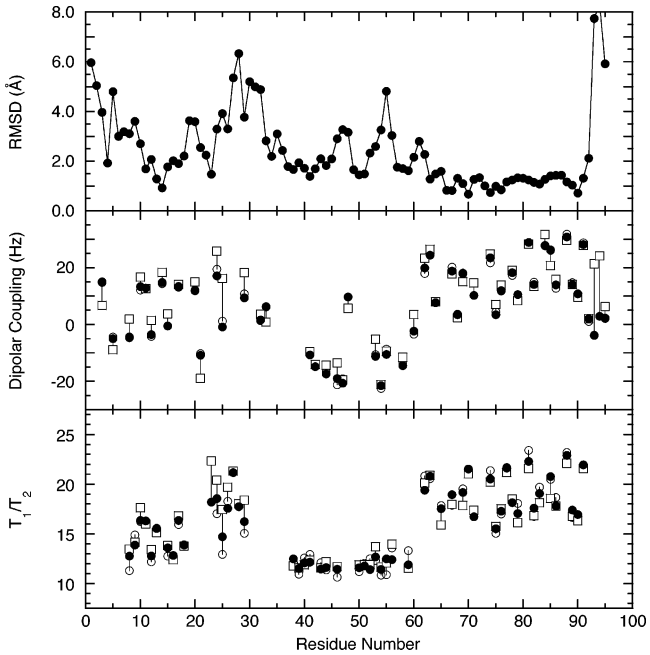

FIGURE 7: Comparison of NMR and crystal structures. The sequence dependence of the rmsd of the backbone atoms of the average NMR structure relative to the X-ray crystal structure (top). The sequence dependence of experimental RDCs (○) is compared to those calculated from the refined NMR structure (●) and the X-ray structure (1R7J) of Sso10a (□) (middle). In addition, the sequence dependence of experimental T_1/T_2 ratios (○) is compared to those calculated from the NMR structure (●) and the X-ray crystal structure (□) (bottom). Vertical lines connect experimental data and values calculated from the crystal structure to indicate locations in the sequence where the NMR data indicate differences in the solution and crystal structures.

Nonetheless, T_1/T_2 relaxation restraints had a significant effect on the final structures and resulted in models with less deviation from the X-ray crystal structure. Using the base NMR restraints, the rmsd between NMR and X-ray structures were 4.2 Å, which decreased to 3.0 and 2.6 Å with inclusion of dipolar coupling and T_1/T_2 restraints, respectively. The best agreement between the NMR and crystal structures (rmsd of 2.2 Å) was obtained when both RDCs and relaxation restraints were utilized.

However, there are significant differences between the NMR and crystal structures as represented by the magnitude of the NMR restraint violations in the crystal structure compared to those for the final NMR structure. The largest deviations occur not only at the ends where the NMR structure is less well-defined and flexibility is indicated by the ^{15}N relaxation data (see above) but also from T24 to L32. This includes the α2 helix, which the ^{15}N relaxation data indicate to be rigid, while the backbone rmsd values indicate some increased imprecision in this region. We conclude that the α2 helix as a unit is well-defined, but its position is somewhat flexible. It is clear from the discrepancies in the observed RDC and T_1/T_2 ratios and those expected from the

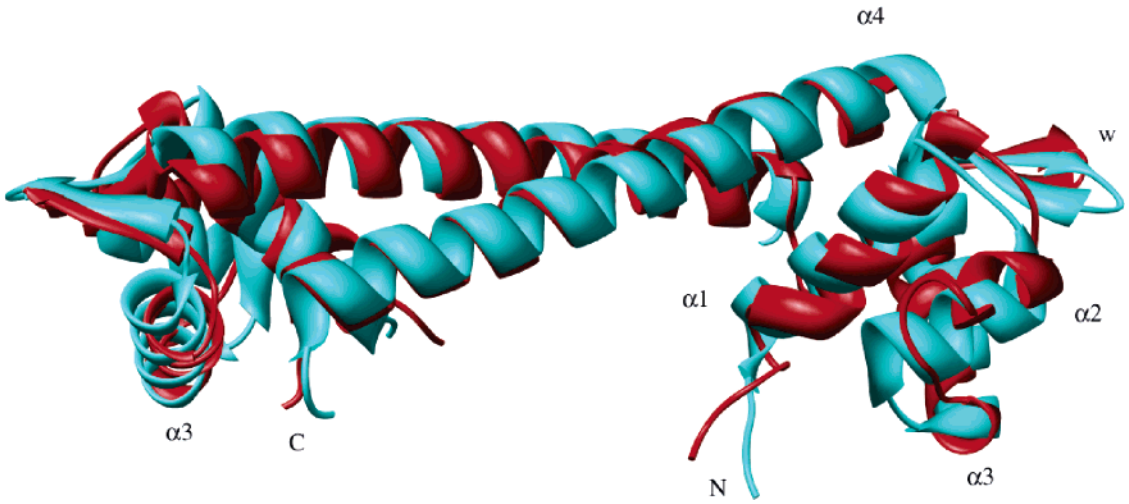

FIGURE 8: Overlay of the NMR solution structure (red) defined with RDC and T_1/T_2 relaxation data onto the X-ray crystal structure (cyan) (*14*). Alignment was performed using backbone atoms in regions of ordered secondary structure (see Figure 4). The four helices as well as the wing are labeled.

X-ray structure (Figure 7) that one of the most significant differences occurs in this region of the protein. This difference is demonstrated in the overlay of the two structures (Figure 8) where the α2 helix in the NMR structure (red) is shorter and tilted away from the α3 helix more than observed in the crystal structure (cyan). No slowly exchanging amide protons were observed in α2, the interconnecting loop, or the first half of α3. We conclude that this region of the molecule is not exceptionally stable and may adopt slightly different conformations under different solvent conditions or because of packing interactions in the crystal. Some degree of adaptability may be necessary in this region for optimal DNA-binding interactions.

DISCUSSION

Sso10a is a dimer of winged helices with the dimer interface largely defined by a solvent-exposed, two-stranded antiparallel coiled coil. Winged helix dimers with an antiparallel coiled coil have been described in a number of DNA regulatory proteins, including replication terminator protein RTP from *Bacillus subtilis* (*38*), the MerR family of metalloregulatory proteins including a zeptomolar copper-sensitive CueR in *E. coli* (*39*, *40*), the molybdate-dependent transcription regulator ModE in *E. coli* (*41*), and the bacteriophage T4 transcription regulator MotA (*42*). The sequential topology of Sso10a is similar to many of these proteins in that the wing occurs between the HTH and coiled-coil C-terminal helix (Figure 9). However, Sso10a differs from most in the packing of the coiled-coil helices and the presence of additional structural elements packed against the coil. The fold and size of the CueR winged helix domains differ significantly from Sso10a.

The positioning of a globular winged helix at the end of a coiled-coil rod in Sso10a leads to the question of independence and freedom of movement at the junctions between the three subdomains. Independent movement of the two winged helices could play an important role in DNA binding by providing flexibility in the positioning of the protein-binding sites on DNA. The NMR structure shows a small difference in the positioning of the winged helices relative to the coiled coil compared to that in the crystal structure (Figure 8), which results from about a 15−20° rotation of the winged helix away from the coil. However, as seen in Figure 8, the effect is small and is on the order of the limit in precision of the NMR and crystal structures. The absence of significant flexibility at the coil-head junction is supported by the consistently high-order parameters on both sides of the interface with almost no need to invoke R_{ex} to fit the ^{15}N relaxation data. In addition, the distribution of high PFs in α1, α2, the wing, and α4 indicates that the interface between the winged helix and the coiled coil is a well-packed and stable hydrophobic core. The N−H of G63 is the most highly protected and lies near the N terminus of the coil helix α4 facing the winged helix subdomain. The totality of the data indicates that the coiled-coil and winged helices constitute a single cooperative domain, an observation which is supported by a single endotherm in the DSC at pH 7 (*14*).

The most significant locus of differences in the NMR and crystal structures of Sso10a appears to occur at the putative DNA-binding HTH region and in particular in the location and length of the α2 helix, i.e., the first helix in the HTH motif (Figure 7). This helix is well-defined by the NMR data. The deviations observed for the observed RDC and T_1/T_2 restraints compared to those calculated from the crystal structure (Figure 7) indicate that the differences in solution and crystal structures are real and not due to limitations in the NMR data. It is interesting to note that protein−protein interactions in the crystal occur not only between the α4 helices but also between residues in the α2 helix and those in the vicinity of E85. It therefore is not surprising that the positions of these segments might differ slightly in the crystal and NMR structures.

The antiparallel coiled-coil structure of dimeric Sso10a has been discussed and compared to other coiled coils elsewhere (*14*). The most surprising aspect of the coiled coil is the apparent lack of optimization of the hydrophobic interface in this hyperthermophile protein. It is interesting therefore that the PFs observed here indicate that the stability of the coil is significant and comparable to that of the winged helix. This is true even in the vicinity of the buried aspartate D69. The acidic D69 side chain is largely buried in both the

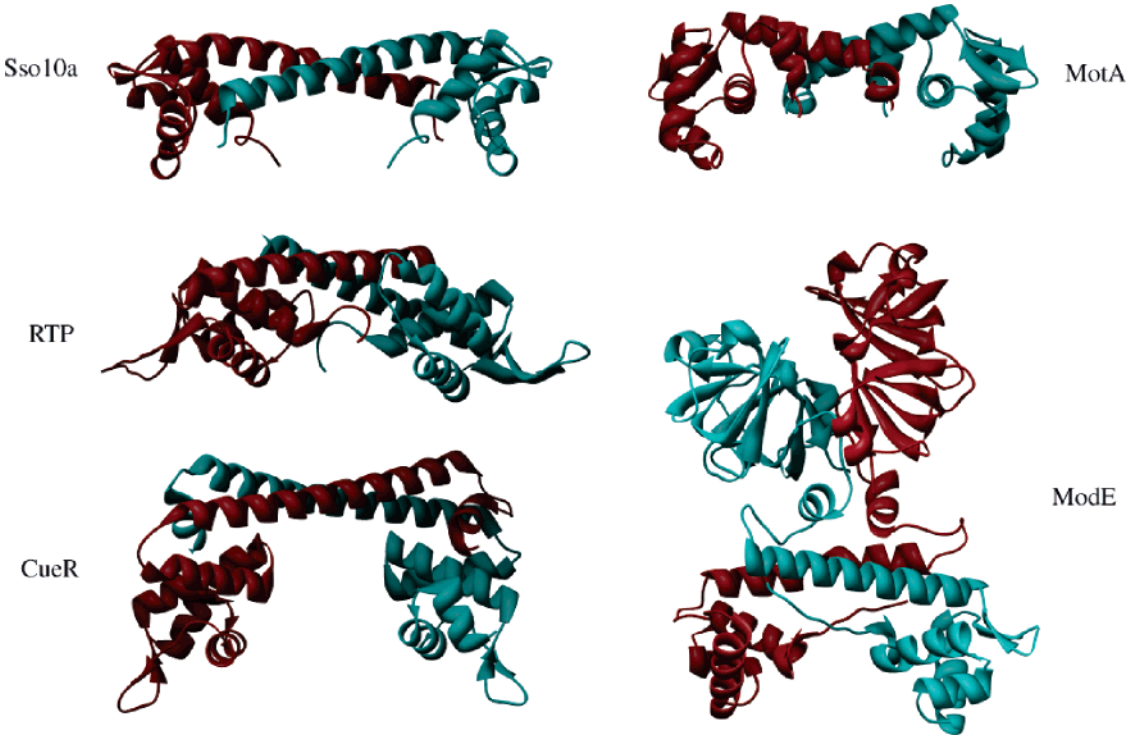

FIGURE 9: Comparison of the structure of Sso10a to four additional examples of winged helix dimers with antiparallel coiled-coil dimerization motifs: RTP (1F4K), replication terminator protein from *Bacillus subtilis* (*38*); CueR (1Q05), a copper-binding regulatory protein from *E. coli* (*40*); MotA (1BJA), a bacteriophage T4 regulatory protein (*42*); and ModE (1B9M), a molybdate-dependent transcription regulator from *E. coli* (*41*). Monomeric subunits are distinguished by cyan and red.

crystal and NMR structures at the hydrophobic interface with only 10% solvent accessibility relative to that in the extended chain. We note that the intermolecular salt bridge (D69-K86) that was well-defined in the crystal structure was not apparent in the solution structure because of the absence of NOEs between the two groups. This may indicate that ion pairing in solution is not as static as indicated by the crystal structure. However, the D69-K86 interactions in solution are important because the K86A substitution significantly destabilizes the dimer (M. Kahsai, unpublished). However, the D69A substitution led to a more thermally stable dimer, indicating that the D69-K86 interaction cannot completely counter the destabilization caused by burying an aspartate at the coil interface.

Location of Conserved Sequences in the Structure. It is interesting to note the positions of those residues that are conserved in the COG3432 group of proteins. G63 is one of the most conserved (100%) of all of the residues. It is buried at the coil-winged helix interface and would appear to permit tight packing of the two subdomains. K62 is solvent-exposed and might be involved in forming a salt bridge with E48 at the end of α3, although this residue is not well-conserved in COG3432. T24, N31, Y34, and Y40 are well-conserved in the helix-turn-helix motif and are likely candidates for specific interactions with DNA.

Finally, we note that the structure of Sso10a defines the location of the single tryptophan in the homologous Sac10a, which is perturbed by DNA binding. Alignment of the Sac10a and Sso10a sequences (*13*) shows that W33 in Sac10a coincides with R25 in the Sso10a sequence, which occurs near the middle of the α2 helix on the solvent-exposed surface of the HTH motif. The increased fluorescence observed upon Sac10a DNA binding (*13*) is consistent with decreased solvent exposure and therefore decreased solvent quenching of the intrinsic tryptophan fluorescence. The fluorescence data therefore supports a model in which the α2 helix is important in DNA binding.

ACKNOWLEDGMENT

The authors acknowledge assistance from Dr. James Prestegard (University of Georgia) in the use of REDCAT and from Dr. Ranjith Muhandiram (University of Toronto) for assistance in installing various NMR pulse sequences, which were generously provided by Dr. Lewis Kay (University of Toronto).

SUPPORTING INFORMATION AVAILABLE

Table provided with the refinement statistics for solution structures obtained using basic NMR constraints alone (NOEs, torsional angle and coupling constant constraints, and hydrogen bonds), and with RDCs and/or T_1/T_2 restraints. This material is available free of charge via the Internet at http://pubs.acs.org.

REFERENCES

1. Dijk, J., and Reinhardt, R. (1986) in *Bacterial Chromatin* (Gualerzi, C., and Pon, C., Eds.) Springer-Verlag, Berlin, Germany.
2. White, M. F., and Bell, S. D. (2002) Holding it together: Chromatin in the archaea, *Trends Genet. 18*, 621−626.
3. Wardleworth, B. N., Russell, R. J., Bell, S. D., Taylor, G. L., and White, M. F. (2002) Structure of Alba: An archaeal chromatin protein modulated by acetylation, *EMBO J. 21*, 4654−4662.
4. Edmondson, S. P., Qiu, L., and Shriver, J. W. (1995) Solution structure of the DNA-binding protein Sac7d from the hyperthermophile *Sulfolobus acidocaldarius*, *Biochemistry 34*, 13289−13304.
5. McAfee, J. G., Edmondson, S., Zegar, I., and Shriver, J. W. (1996) Equilibrium DNA binding of Sac7d protein from the hyperther-

mophile *Sulfolobus acidocaldarius*: Fluorescence and circular dichroism studies, *Biochemistry 35*, 4034−4045.
6. Lundback, T., and Hard, T. (1996) Salt dependence of the free energy, enthalpy, and entropy of nonsequence specific DNA binding, *J. Phys. Chem. 100*, 17690−17695.
7. Robinson, H., Gao, Y.-G., McCrary, B. S., Edmondson, S. P., Shriver, J. W. and Wang, A. H.-J. (1998) The hyperthermophile chromosomal protein Sac7d sharply kinks DNA, *Nature 392*, 202−205.
8. McCrary, B. S., Bedell, J., Edmondson, S. P., and Shriver, J. W. (1998) Linkage of protonation and anion binding to the folding of Sac7d, *J. Mol. Biol. 276*, 203−224.
9. Lundback, T., Hansson, H., Knapp, S., Ladenstein, R., and Hard, T. (1998) Thermodynamic characterization of non-sequence-specific DNA-binding by the Sso7d protein from *Sulfolobus solfataricus*, *J. Mol. Biol. 276*, 775−786.
10. Edmondson, S. P., and Shriver, J. W. (2001) DNA binding proteins Sac7d and Sso7d from *Sulfolobus*, *Methods Enzymol. 334*, 129−145.
11. Clark, A. T., McCrary, B. S., Edmondson, S. P., and Shriver, J. W. (2004) Thermodynamics of core hydrophobicity and packing in the hyperthermophile proteins Sac7d and Sso7d, *Biochemistry 43*, 2840−2853.
12. Peters, W. B., Edmondson, S. P., and Shriver, J. W. (2004) Thermodynamics of DNA binding and distortion by the hyperthermophile chromatin protein sac7d, *J. Mol. Biol. 343*, 339−360.
13. Edmondson, S. P., Kahsai, M. A., Gupta, R., and Shriver, J. W. (2004) Characterization of Sac10a, a hyperthermophile DNA-binding protein from *Sulfolobus acidocaldarius*, *Biochemistry 43*, 13026−13036.
14. Chen, L., Chen, L. R., Zhou, X. E., Wang, Y., Kahsai, M. A., Clark, A. T., Edmondson, S. P., Liu, Z. J., Rose, J. P., Wang, B. C., Meehan, E. J., and Shriver, J. W. (2004) The hyperthermophile protein Sso10a is a dimer of winged helix DNA-binding domains linked by an antiparallel coiled coil rod, *J. Mol. Biol. 341*, 73−91.
15. Lurz, R., Grote, M., Dijk, J., Reinhardt, R., and Dobrinski, B. (1986) Electron microscopic study of DNA complexes with proteins from the archaebacterium *Sulfolobus acidocaldarius*, *EMBO J. 5*, 3715−3721.
16. Lupas, A. (1996) Prediction and analysis of coiled-coil structures, *Methods Enzymol. 266*, 513−525.
17. Teale, M., Kahsai, M., Singh, S. K., Edmondson, S. P., Gupta, R., Shriver, J. W., and Meehan, E. (2003) Cloning, expression, crystallization, and preliminary X-ray analysis of the DNA-binding protein Sso10a from *Sulfolobus solfataricus*, *Acta Crystallogr., Sect. D 59*, 1320−1322.
18. Kawarabayasi, Y., Hino, Y., Horikawa, H., Jin-no, K., Takahashi, M., Sekine, M., Baba, S., Ankai, A., Kosugi, H., Hosoyama, A., Fukui, S., Nagai, Y., Nishijima, K., Otsuka, R., Nakazawa, H., Takamiya, M., Kato, Y., Yoshizawa, T., Tanaka, T., Kudoh, Y., Yamazaki, J., Kushida, N., Oguchi, A., Aoki, K., Masuda, S., Yanagii, M., Nishimura, M., Yamagishi, A., Oshima, T., and Kikuchi, H. (2001) Complete genome sequence of an aerobic thermoacidophilic crenarchaeon, *Sulfolobus tokodaii* strain 7, *DNA Res. 8*, 123−140.
19. Gill, S., and von Hippel, P. (1989) Calculation of protein extinction coefficients from amino acid sequence data, *Anal. Biochem. 182*, 319−326.
20. Delaglio, F., Grzesiek, S., Vuister, G. W., Zhu, G., Pfeifer, J., and Bax, A. (1995) NMRPipe: A multidimensional spectral processing system based on UNIX pipes, *J. Biomol. NMR 6*, 277−293.
21. Johnson, B. A. (2004) Using NMRView to visualize and analyze the NMR spectra of macromolecules, *Methods Mol. Biol. 278*, 313−352.
22. Tollinger, M., Crowhurst, K. A., Kay, L. E., and Forman-Kay, J. D. (2003) Site-specific contributions to the pH dependence of protein stability, *Proc. Natl. Acad. Sci. U.S.A. 100*, 4545−4550.
23. Kuboniwa, H., Grzesiek, S., Delaglio, F., and Bax, A. (1994) Measurement of HN−H α J couplings in calcium-free calmodulin using new 2D and 3D water-flip-back methods, *J. Biomol. NMR 4*, 871−878.
24. Zwahlen, C., Legault, P., Vincent, S. J. F., Greenblatt, J., Konrat, R., and Kay, L. E. (1997) Methods for measurement of intermolecular NOEs by multinuclear NMR spectroscopy: Application to a bacteriophage λ N-peptide/boxB RNA complex, *J. Am. Chem. Soc. 119*, 6711−6721.
25. Ruckert, M., and Otting, G. (2000) Alignment of biological macromolecules in novel nonionic liquid crystalline media for NMR experiments, *J. Am. Chem. Soc. 122*, 7793−7797.
26. Farrow, N. A., Muhandiram, R., Singer, A. U., Pascal, S. M., Kay, C. M., Gish, G., Shoelson, S. E., Pawson, T., Forman-Kay, J. D., and Kay, L. E. (1994) Backbone dynamics of a free and phosphopeptide-complexed Src homology 2 domain studied by ^{15}N NMR relaxation, *Biochemistry 33*, 5984−6003.
27. Korzhnev, D. M., Skrynnikov, N. R., Millet, O., Torchia, D. A., and Kay, L. E. (2002) An NMR experiment for the accurate measurement of heteronuclear spin-lock relaxation rates, *J. Am. Chem. Soc. 124*, 10743−10753.
28. Mandel, A. M., Akke, M., and Palmer, A. G., III (1995) Backbone dynamics of *Escherichia coli* ribonuclease HI: Correlations with structure and function in an active enzyme, *J. Mol. Biol. 246*, 144−163.
29. Linge, J. P., O'Donoghue, S. I., and Nilges, M. (2001) Automated assignment of ambiguous nuclear overhauser effects with ARIA, *Methods Enzymol. 339*, 71−90.
30. Brunger, A. T., Adams, P. D., Clore, G. M., DeLano, W. L., Gros, P., Grosse-Kunstleve, R. W., Jiang, J. S., Kuszewski, J., Nilges, M., Pannu, N. S., Read, R. J., Rice, L. M., Simonson, T., and Warren, G. L. (1998) Crystallography & NMR system: A new software suite for macromolecular structure determination, *Acta Crystallogr., Sect. D 54* (part 5), 905−921.
31. Valafar, H., and Prestegard, J. H. (2004) REDCAT: A residual dipolar coupling analysis tool, *J. Magn. Reson. 167*, 228−241.
32. Schwieters, C. D., Kuszewski, J. J., Tjandra, N., and Marius Clore, G. (2003) The Xplor-NIH NMR molecular structure determination package, *J. Magn. Reson. 160*, 65−73.
33. Bai, Y., Milne, J. S., Mayne, L., and Englander, S. W. (1994) Protein stability parameters measured by hydrogen exchange, *Proteins 20*, 4−14.
34. Lipari, G., and Szabo, A. (1982) Model-free approach to the interpretation of nuclear magnetic resonance relaxation in macromolecules, *J. Am. Chem. Soc. 104*, 4546−4559.
35. Adamson, J. G., Zhou, N. E., and Hodges, R. S. (1993) Structure, function, and application of the coiled-coil protein folding motif, *Curr. Opin. Biotechnol. 4*, 428−437.
36. Lupas, A. (1996) Coiled coils: New structures and new functions, *Trends Biochem. Sci. 21*, 375−382.
37. Oakley, M. G., and Hollenbeck, J. J. (2001) The design of antiparallel coiled coils, *Curr. Opin. Struct. Biol. 11*, 450−457.
38. Bussiere, D. E., Bastia, D., and White, S. W. (1995) Crystal structure of the replication terminator protein from *B. subtilis* at 2.6 Å, *Cell 80*, 651−660.
39. Godsey, M. H., Zheleznova Heldwein, E. E., and Brennan, R. G. (2002) Structural biology of bacterial multidrug resistance gene regulators, *J. Biol. Chem. 277*, 40169−40172.
40. Changela, A., Chen, K., Xue, Y., Holschen, J., Outten, C. E., O'Halloran, T. V., and Mondragon, A. (2003) Molecular basis of metal-ion selectivity and zeptomolar sensitivity by CueR, *Science 301*, 1383−1387.
41. Hall, D. R., Gourley, D. G., Leonard, G. A., Duke, E. M., Anderson, L. A., Boxer, D. H., and Hunter, W. N. (1999) The high-resolution crystal structure of the molybdate-dependent transcriptional regulator (ModE) from *Escherichia coli*: A novel combination of domain folds, *EMBO J. 18*, 1435−1446.
42. Finnin, M. S., Cicero, M. P., Davies, C., Porter, S. J., White, S. W., and Kreuzer, K. N. (1997) The activation domain of the MotA transcription factor from bacteriophage T4, *EMBO J. 16*, 1992−2003.

BI047669T